SCIENCE CHINA
Earth Sciences

• RESEARCH PAPER •

February 2016 Vol.59 No.2: 320–327
doi: 10.1007/s11430-015-5146-y

Measurement of aerosol effective density by single particle mass spectrometry

ZHANG GuoHua[1], BI XinHui[1*], HAN BingXue[1,2], QIU Ning[3], DAI ShouHui[2], WANG XinMing[1], SHENG GuoYing[1] & FU JiaMo[1]

[1] *Guangzhou Institute of Geochemistry, Chinese Academy of Sciences, Guangzhou 510640, China;*
[2] *College of Earth Science, University of Chinese Academy of Sciences, Beijing 100049, China;*
[3] *South China Sea Institute of Oceanology, Chinese Academy of Sciences, Guangzhou 510301, China*

Received February 10, 2015; accepted May 15, 2015; published online July 31, 2015

Abstract Single particle mass spectrometry has been widely used to determine the size and chemical compositions of atmospheric aerosols; however, it is still rarely used for the microphysical properties measurement. In this study, two methods were developed for determining aerosol effective density by a single particle aerosol mass spectrometer (SPAMS). Method I retrieved effective density through comparison between measured light scattering intensities and Mie theoretical modelled partial scattering cross section. Method II coupled a differential mobility analyzer (DMA) with SPAMS to simultaneously determine the electric mobility and vacuum aerodynamic diameter, and thus the effective density. Polystyrene latex spheres, ammonium sulfate and sodium nitrate were tested by these methods to help validate their effectiveness for determining the aerosol effective density. This study effectively extends SPAMS measurements to include particle size, chemical composition, light scattering, and effective density, and thus helps us better understand the environment and climate effects of aerosols.

Keywords Effective density, Single particle, SPAMS, Mie theory, DMA

Citation: Zhang G H, Bi X H, Han B X, Qiu N, Dai S H, Wang X M, Sheng G Y, Fu J M. 2016. Measurement of aerosol effective density by single particle mass spectrometry. Sci China Earth Sci, 59: 320−327, doi: 10.1007/s11430-015-5146-y

1. Introduction

Atmospheric aerosols have significant effects on regional environmental pollution, global climate, and human health (Pöschl, 2005). Aerosols will undergo coagulation, heterogeneous reactions, gas-to-particle partitioning, and in-cloud processing during long-range transport after emission, which would lead to changes of particle size, structure, and chemical composition (Zhu et al., 2011; Pöschl, 2005). The complex nature and ever-changing physiochemical properties of atmospheric aerosols introduce large uncertainties in quantifying their effects on environment, climate, and human health.

Traditional single particle analysis instruments, such as the scanning electron microscopy (SEM) and transmission electron microscopy (TEM), coupled with energy dispersive X-ray microanalyses (EDX) are capable of measuring the morphological, physical, and chemical properties of particles. However, these methods suffer from some artifacts, such as evaporation and chemical reactions of particles during sample collection, storage and analysis (Bzdek et al., 2012; Lee and Allen, 2012). Single Particle Mass Spectrometry (SPMS) provides real-time size and chemical composition data for individual aerosol particles (Li et al., 2011; Prather et al., 1994). The development and application of SPMS during the past decades improve insight into gas-particle partitioning, heterogeneous reactions, and par-

*Corresponding author (email: bixh@gig.ac.cn)

ticle sources (Creamean et al., 2013; Pratt and Prather, 2012). The SPMS measurement has recently been extended to include the particle size, chemical composition, shape, effective density, refractive index, volatility, and hygroscopicity (Buzorius et al., 2002; Pratt and Prather, 2009; Spencer et al., 2007; Zelenyuk et al., 2008). However, the understanding of the properties of single particles in China is still limited. The reported studies focus on the measurements of mixing state of atmospheric aerosols, the formation mechanisms of secondary species in urban areas (e.g., Yang et al., 2009, 2012), and the formation of secondary organic aerosols in a chamber (Liang et al., 2005; Wang et al., 2006; Xia et al., 2004). Additionally, a commercialized single particle aerosol mass spectrometer (SPAMS) has also been developed (Huang et al., 2010; Li et al., 2011) and applied to on-line detection of single particles in the ambient atmosphere or directly from emission sources (e.g., He et al., 2013; Li et al., 2013). However, only the size and chemical compositions of single particles were analyzed in these studies.

Particle density is an important parameter and is generally represented with the term effective density (ρ_{eff}). The ρ_{eff} is used to distinguish between true particle density and a measured one that is dependent on true density and shape (DeCarlo et al., 2004). One of the most common approaches is to simultaneously measure electrical mobility diameter (d_{m}) by a differential mobility analyzer (DMA) and particle mass by an electrical low-pressure impactor (ELPI) or aerosol particle mass analyzer (APM) (Van Gulijk et al., 2004; Virtanen et al., 2006). However, the calculated density is an average of the ensemble of particles irrespective of their compositions or sizes. In the present study, two methods were developed for the measurement of ρ_{eff} by SPAMS, which was improved with light scattering measurement module in Method I and was coupled with a DMA in Method II. Thus, the measurements of SPAMS are extended to include particle size, chemical compositions, effective density, and light scattering.

2. Method

2.1 SPAMS

Single particle detection procedure with SPAMS can be found elsewhere (Huang et al., 2010; Li et al., 2011). Briefly, aerosol individual particle is drawn into aerodynamic lens of SPAMS through a 0.1 mm critical orifice. Velocity of the particle is determined subsequently by the two continuous diode Nd:YAG laser beams (532 nm). A light scattering measurement module embedded simultaneously records the light scattering signals (LSS) for the particle. The particle is then desorped/ionized by a pulsed Nd:YAG laser (266 nm) triggered exactly based on its velocity. The positive and negative fragments generated are obtained. Overall, particle velocity, LSS, and mass spectra are simultaneously determined. The particle velocity is then corresponded to vacuum aerodynamic diameter (d_{va}) through their linear relationship experimentally determined using a series of standard polystyrene latex spheres (PSL, Nanosphere Size Standards, Duke Scientific Corp., Palo Alto) with predefined sizes.

2.2 DMA

Aerosols were dried with a Nafion membrane dryer prior to the size selection. The aerosols are then neutralized before entering the DMA (Model 1500 Aerosol Generation and Monitoring System, MSP cooperation, MN, USA) to achieve a nearly Boltzmann distribution of charges. Highly monodisperse particles with a series of specific d_{m} were outputted by controlling the voltage in the DMA. The sample air and sheath air flows were held at 0.3 and 3 L min^{-1}, respectively.

2.3 Method testing

In the present study, PSL, ammonium sulfate, and sodium nitrate were tested to validate the measurement of SPAMS and DMA-SPAMS. The samples were dissolved in ultrapure water (Milli-Q Grandient, Millipore Company, USA) for aerosol generation. The aerosols generated by an aerosol generation system (Model 1500 Aerosol Generation and Monitoring System, MSP cooperation, MN, USA) were introduced into SPAMS after dried.

2.4 Theoretical calculations

Mie theory describes the scattering of electromagnetic radiation by a sphere, and has been widely applied in light extinction properties of atmospheric aerosols (Lin et al., 2013). The partial scattering cross section (PSCS, R_{SPAMS}) can be described as:

$$R_{\text{theory}} = \frac{1}{k^2}\iint (|S1|^2 \sin^2\phi + |S2|^2 \cos^2\phi)\sin\theta \mathrm{d}\theta \mathrm{d}\phi, \quad (1)$$

where k is the wavenumber, expressed as $2\pi/\lambda$ (λ is the wavelength of the light source, λ=532 nm in the present study). ϕ is the azimuth angle from the plane of polarization, θ is the polar angle. The scattering amplitude matrix elements are expressed as $S1$ and $S2$, as a function of the refractive index (expressed as real refractive index n for scattering calculation), particle size (d_{p}), λ, and θ. The refractive index is given by $n+i\times k$ with n and k being real constants and $i=(-1)^{1/2}$. The integral of eq. (1) is evaluated over the angular range for which the light was collected by the SPAMS light collection mirror.

The particle size d_{p} can be approximately expressed as a function of d_{va} that measured by SPAMS in the present study:

$$d_{va} = d_p \frac{\rho_p}{\chi \cdot \rho_0}. \quad (2)$$

where ρ_p is known as the material density; ρ_0 is the standard density (1.0 g cm^{-3}); χ is the dynamic shape factor. In addition, the effective density is introduced to further simplify the function (DeCarlo et al., 2004; Hand and Kreidenweis, 2002; Khlystov et al., 2004):

$$\rho_{eff}^{I} = \frac{\rho_p}{\chi}. \quad (3)$$

For spherical particles, χ=1, ρ_{eff}=ρ_p; for non-spherical particles, ρ_{eff} <ρ_p.

From eqs. (1)–(3), the PSCS (R_{SPAMS}) can be expressed as a function of n and ρ_{eff}.

2.5 Determination of effective density with DMA-SPAMS

The methodology for the determination of effective density by DMA-SPAMS has been described in published literature (Spencer et al., 2007; Zelenyuk et al., 2008). Monodisperse particles with specific d_m (200–600 nm for ammonium sulfate and sodium nitrate, uncertainty within 1%) selected by DMA were introduced into SPAMS to measure their d_{va}. The ρ_{eff} could be then calculated by (DeCarlo et al., 2004; Moffet et al., 2008):

$$\rho_{eff}^{II} = \frac{d_{va}}{d_m} \cdot \rho_0. \quad (4)$$

3. Results and discussion

3.1 Relationship between measured light scattering intensities and PSCS

PSL (ρ_p=1.054 g cm^{-3}, n=1.59) (Nanosphere Size Standards, Duke Scientific Corp., Palo Alto) of a series of pre-defined sizes (0.15, 0.3, 0.5, 0.72, 1.0, 2.0 μm) were used as standard spherical particles to build the relationship between the measured LSS and PSCS, in order to compare the light scattering measurements of SPAMS with Mie theory. The upper limit (90th percentile) value was used in the comparison, because it represents the scattering that occurs between well located spherical particles and laser beam (Moffet and Prather, 2005; Moffet et al., 2008). A well fitted linear relationship (R^2=0.95) is obtained (Figure 1) and could be applied to make conversion between measured LSS and PSCS for ambient aerosols.

3.2 Least Square error method for retrieving n and ρ_{eff} for ambient aerosols

The measured LSS were first binned by size (bin width=20 nm), and then the upper-limit values excluding outliers were calculated for each size bin. The light scattering intensities can be transformed into PSCS to build scattering curves, as a function of d_{va}. The square error between the transformed and theoretical PSCS can be calculated by:

$$\text{Square error} = \sum_1^n (R_{trans} - R_{theory})^2. \quad (5)$$

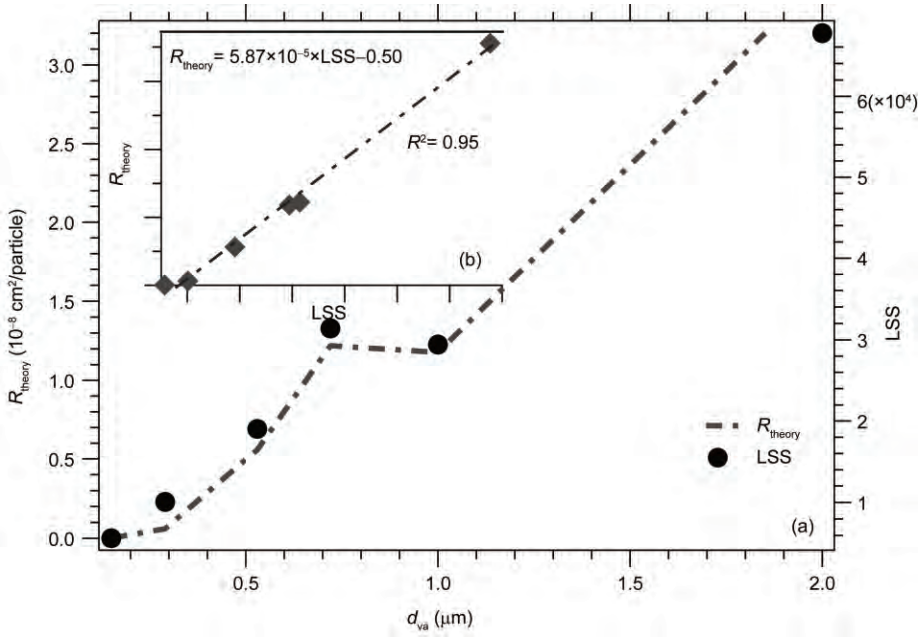

Figure 1 Upper limit of LSS and theoretical PSCS for PSL as a function of size (0.15, 0.3, 0.5, 0.72, 1, and 2 μm) (a) and their relationship (b).

Through varying the dependent parameters, i.e., n (1.3–1.6) and ρ_{eff} (1–2.2 g cm^{-3}), it is possible to find a global minimum (LSE, Least Square Error) between the measured and theoretical PSCS. Before performing such analysis, an ART-2a (Adaptive resonance theory) clustering analysis was run to separate samples on the basis of chemical compositions (Moffet et al., 2008). Thus, a set of n and ρ_{eff} could be retrieved for each particle type.

Square error between measured and Mie theoretical PSCS shows that a range of combinations of effective density and refractive index could be the reasonable values for ammonium sulfate and sodium nitrate (Figure 2). This is because the detected particles have a relatively narrow size range to make a comparison between measured and Mie theoretical PSCS (Moffet et al., 2008). However, the detected ambient particles in the present study exhibited a relatively broad distribution of particle size and thus both the n and ρ_{eff} can be retrieved within a narrow range. Fortunately, when a theoretical refractive index is applied in the calculation, i.e., 1.52 for ammonium sulfate and 1.34 for sodium nitrate particles, the retrieved effective densities are 1.53–1.63 g cm^{-3} and 2.0–2.15 g cm^{-3} (Figure 3), respectively, which are slightly lower than their physical density (ρ_p=1.76 g cm^{-3} and 2.26 g cm^{-3}, respectively), attributed to the non-spherical shape (χ>1, eq. (2)). This result indicates that this method could also be suitable for nearly spherical particles.

3.3 Determination of effective density by DMA-SPAMS

Figure 4 shows the d_{va} distributions of ammonium sulfate and sodium nitrate with specific d_m selected by the DMA. It is necessary to note that multiply charged particles may be selected by the DMA, having the same d_m but different d_{va}. (Spencer et al., 2007; Zelenyuk et al., 2005, 2008). This issue could be addressed through the equation:

$$\frac{d_p}{N} = \frac{2C(d_p VL)}{3\mu q_s \ln\left(\frac{R_o}{R_i}\right)}, \quad (6)$$

where, N and $C(d_p)$ refer to the number of charges and Cunningham slip factor, respectively; V, L, R_i and R_o refer

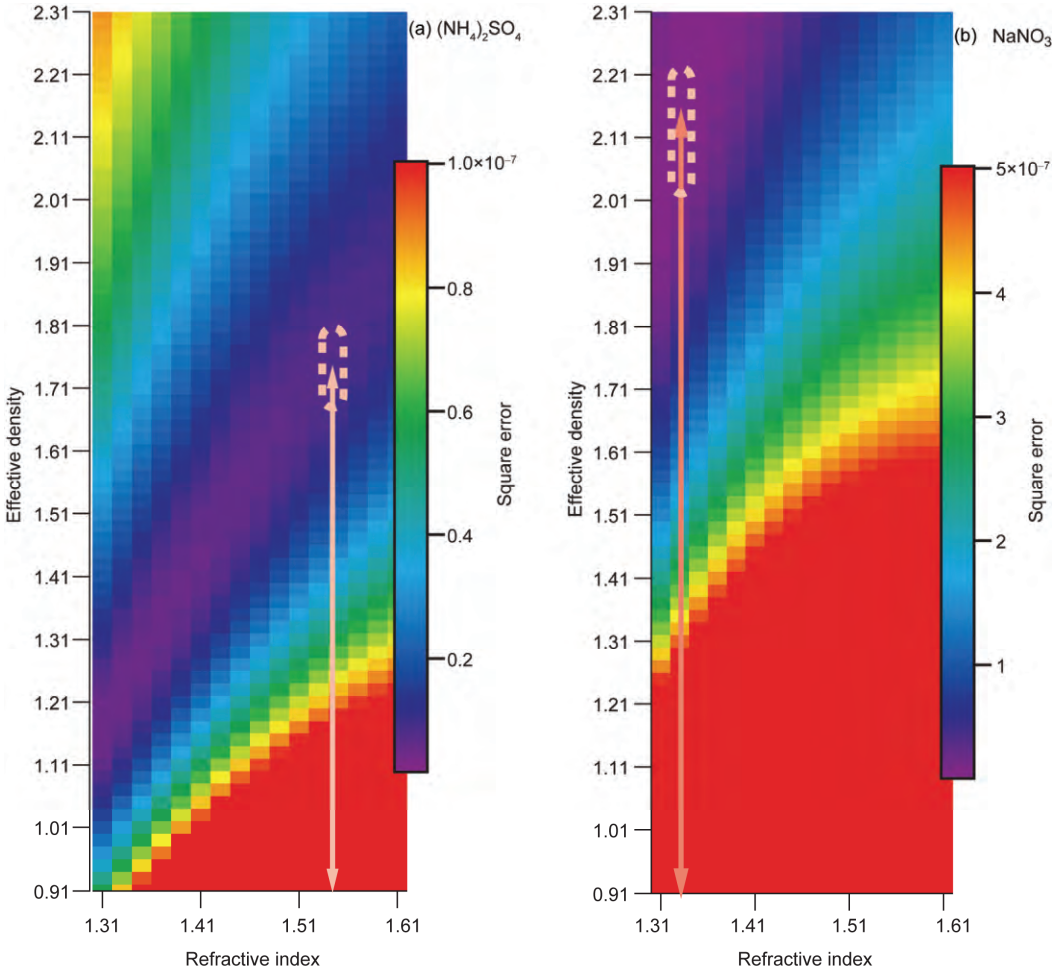

Figure 2 Square error between measured and Mie theoretical PSCS for (a) ammonium sulfate and (b) sodium nitrate.

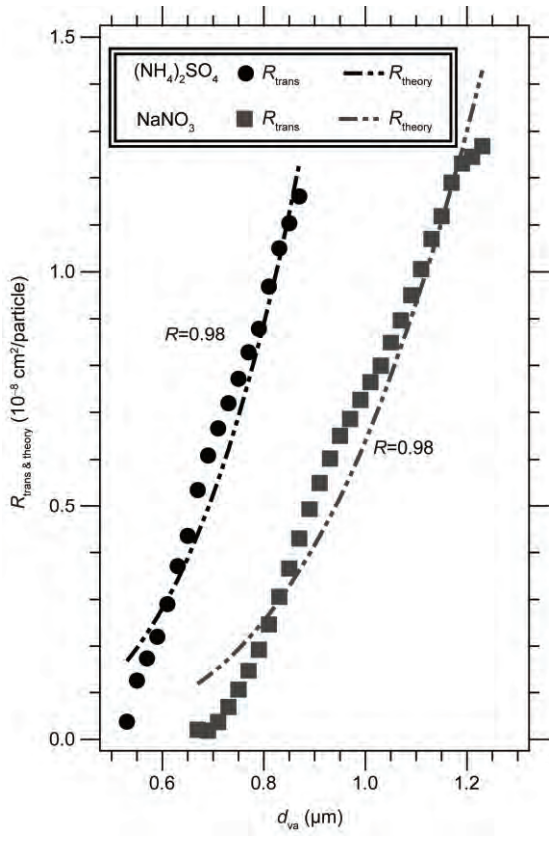

Figure 3 Measured and theoretical PSCS as a function of d_{va} for ammonium sulfate and sodium nitrate.

to the DMA voltage (V), rod length (cm), inner and outer radius (cm) of the DMA annular space, respectively; μ and q_s are gas viscosity (Pa s) and sheath flow (m s^{-1}), respectively. If the number of charges on a particle equals one, then d_p will be equal to d_m. For charges greater than one, d_p will be larger than d_m.

The distribution of ρ_{eff} for ammonium sulfate and sodium nitrate along d_m, calculated from eq. (4), is shown in Figure 5. The uncertainty for ρ_{eff} is estimated from full width at half maximum of the detected peaks in Figure 4. The estimated ρ_{eff} is 1.39–1.54 g cm^{-3} with uncertainty at 8%–12% for ammonium sulfate; and is 1.85–1.99 g cm^{-3} with uncertainty at 8%–13% for sodium nitrate. A similar test by Zelenyuk et al. (2005) obtained ρ_{eff} at 1.6±0.03 and 2.1±0.01 g cm^{-3} for ammonium sulfate and sodium nitrate, respectively. The difference of ρ_{eff} along d_m is attributed to particle shape, transmission efficiency of SPAMS, and systematic errors. Overall, the observed ρ_{eff} exhibits a decrease trend with increasing d_m, due to much more fraction irregular particles in larger sizes (Zelenyuk et al., 2006). The observed ρ_{eff} with this method is lower than those from Mie modelling. This is probably because the ρ_{eff} retrieved from Mie modelling is based on the upper limit of LSS, and thus represents nearly spherical particles. Differently, the observed ρ_{eff} with DMA-SPAMS represents the average ρ_{eff} for all the particles. It is worth noting that DMA-SPAMS could measure a series of ρ_{eff} for particles with varying d_{va}.

3.4 An estimation of the dynamic shape factor

It is possible to further calculate χ for ammonium sulfate and sodium nitrate, through the combination of the obtained ρ_{eff} and their physical densities. The retrieved ρ_{eff} was substituted into eq. (3) to get χ; while the ρ_{eff} obtained by DMA-SPAMS is substituted into the following equation get χ_v (DeCarlo et al., 2004; Spencer et al., 2007):

$$\chi_v = \left(\frac{\rho_p}{\rho_{eff}^{II}} \right)^{\frac{2}{3}}. \quad (7)$$

The result of the estimated χ is summarized in Table 1. It shows that χ_v from DMA-SPAMS is slightly larger than that from Mie modelling, which is consistent with the previous result (Zelenyuk et al., 2006). Similarly, the estimated ρ_{eff} for Mie modelling is larger in former Section 2.3 since the particles inputted in the model represent more spherical shape with χ close to 1.

3.5 Implication for ambient measurements

These two methods are further applied in the analysis of ambient aerosols in Guangzhou urban area. The distributions of d_{va} and chemical compositions for particles with d_m=350 nm, measured by DMA-SPAMS, are displayed in Figure 6. According to the theoretical calculation with the consideration of the number of charges, the estimated ρ_{eff} for particles with d_{va} in the range of four peaks are 0.79, 1.06, 1.32, and 1.56 g cm^{-3}, respectively. This is consistent with the chemical composition for particles with different d_{va}, which is obtained from clustering of mass spectra measured by SPAMS (Sullivan and Prather, 2005). Particles with d_{va} around 470±50 nm were composed of OC as a major component and thus had a relatively lower ρ_{eff} at 0.79 g cm^{-3}. The estimated ρ_{eff} increases with particle d_{va}, because of the increasing fraction of metal content. Additionally, the

Table 1 The estimated dynamic shape factor for ammonium sulfate and sodium nitrate [a)]

	χ (Mie)	χ_v (DMA-SPAMS)	Literatures
Ammonium sulfate	1.11±0.05	1.13±0.03*	1.045–1.06 (Zelenyuk et al., 2006)
Sodium nitrate	1.09±0.06	1.13±0.02	1.07 (Zelenyuk et al., 2005)

a) d_m=200–400 nm; * Averaged over all the selected sizes.

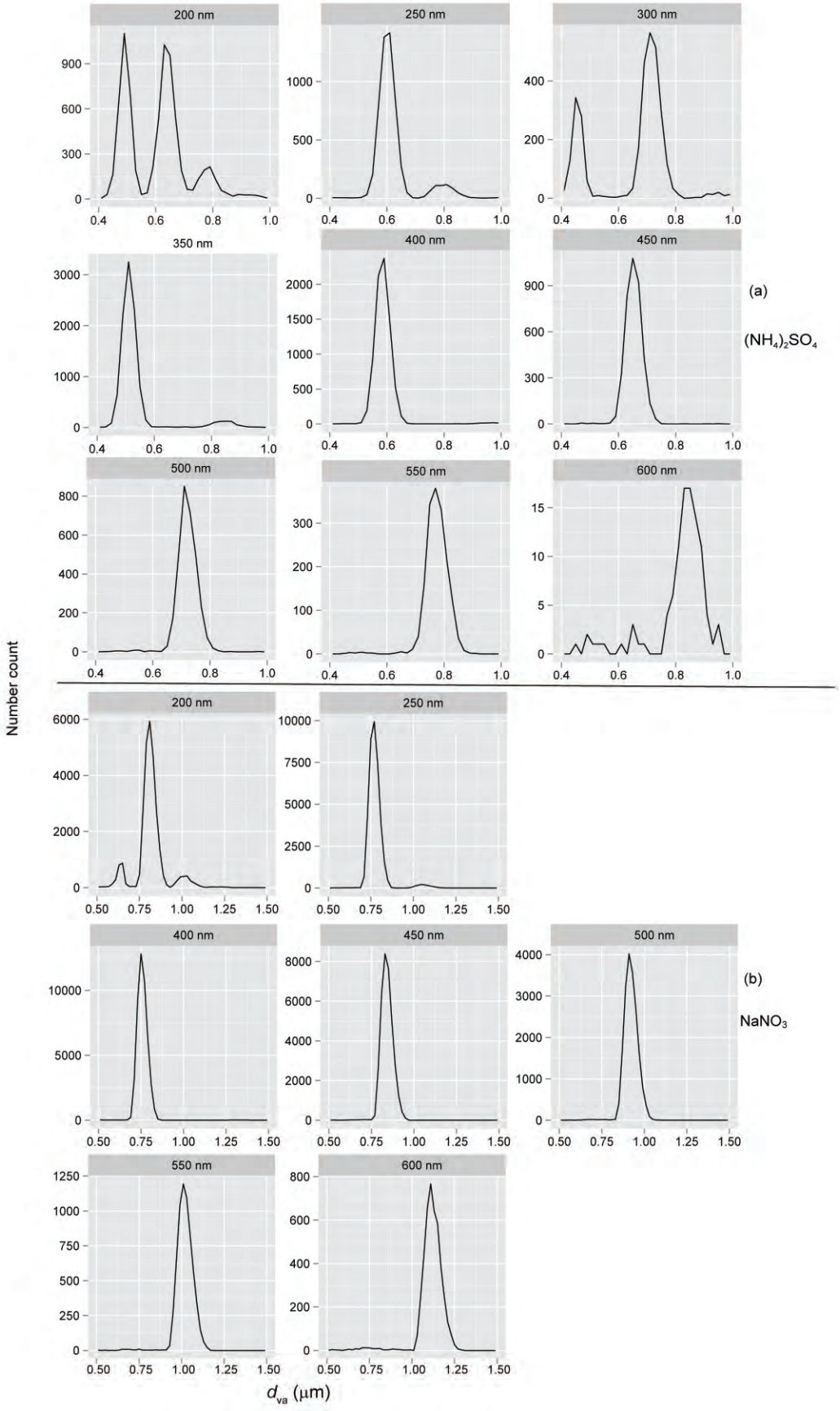

Figure 4 SPAMS d_{va} distributions of (a) ammonium sulfate and (b) sodium nitrate with specific d_m selected by the DMA.

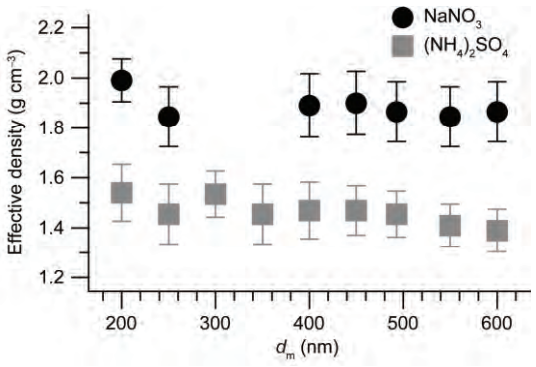

Figure 5 Estimated effective density for ammonium sulfate and sodium nitrate at a series of d_m.

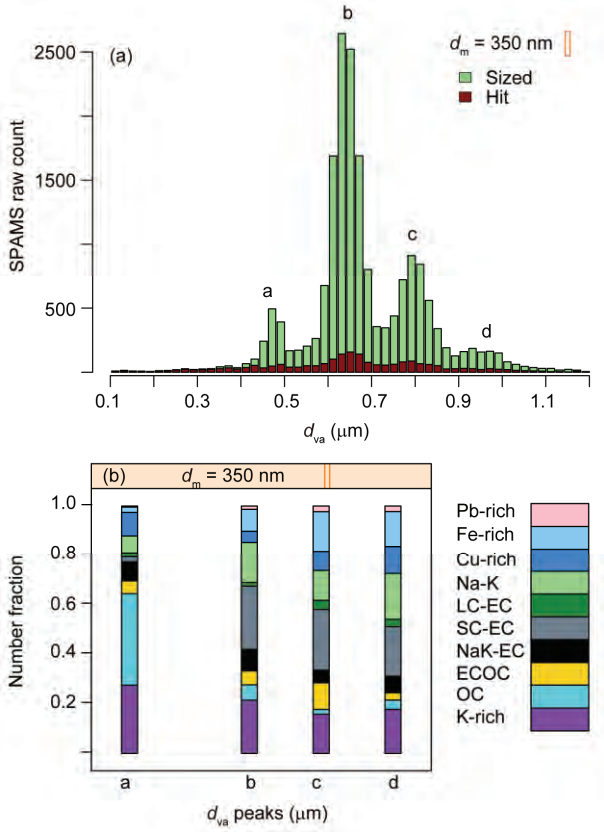

Figure 6 d_{va} distributions for ambient aerosols with d_m=350 nm (a) and their chemical compositions around the d_{va} peaks (±50 nm) (b). Sized and Hit refer to the particle that sized and hit with mass spectra, respectively. According to characteristics of the measured mass spectra, the particles were clustered into several particle types with different chemical composition (Zhang et al., 2013), including potassium rich (K-rich), organics dominated (OC), elemental EC dominated (SC-EC, LC-EC, NaK-EC), internally mixed OC and EC (ECOC), sodium and potassium rich (Na-K), and metal rich Cu-rich, Fe-rich, Pb-rich) types.

illustration of square error distribution versus n and ρ_{eff} in change of particle shape due to particle size might also be a reason.

Two examples are illustrated herein to show the capability of SPAMS in the estimation of n and ρ_{eff}. The LSS obtained for particle types with segregated chemical compositions are inputted in the model to retrieve the n and ρ_{eff}. An

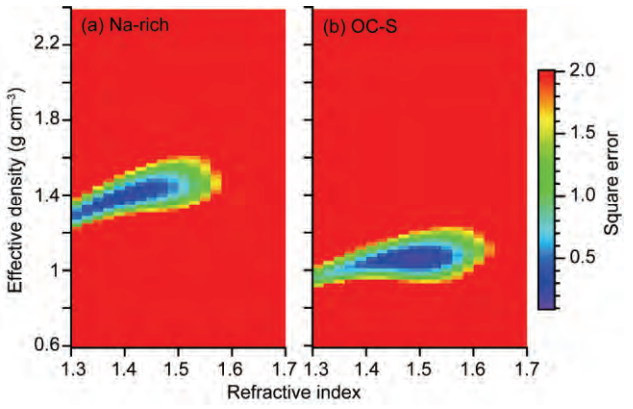

Figure 7 Square error between measured and Mie theoretical PSCS for (a) Na-rich and (b) internally mixed OC and sulfate under a series of given refractive indices (1.3–1.7) and effective densities (0.6–2.4 g cm^{-3}).

illustration of square error distribution versus n and ρ_{eff} in Figure 7 indicates n=1.41±0.04 and ρ_{eff}=1.41±0.04 g cm^{-3} for Na-rich type (typically representing sea salt particles in the atmosphere), while n=1.53±0.04 and ρ_{eff}=1.07±0.02 g cm^{-3} for OC type. As previously noted, it is able to simultaneously retrieve n and ρ_{eff} when the measured d_{va} size range is wide enough (Moffet et al., 2008). Experimental results by Zelenyuk et al. (2006) indicate that NaCl particles of cubic crystalline have ρ_{eff} in a range of 1.6–2.0 g cm^{-3}, decreasing with increasing particle sizes. From the chemical compositions, the observed Na-rich particles have been through some degree of atmospheric ageing, with certain amount of NaCl transformed to be $NaNO_3$. Therefore the observed lower ρ_{eff} for Na-rich type than the crystal type might be attributed to change of particle shape and chemical composition during atmospheric ageing. A similar observation by Moffet et al. (2008) showed n=1.44 and ρ_{eff}=1.38 g cm^{-3} for OC type in the atmosphere of California, which is different from the OC type of Guangzhou atmosphere in this study. It is probably explained by the different chemical compositions of OC between two urban areas.

4. Conclusions

This study effectively extends the analysis capabilities of SPAMS, making it possible to simultaneously measure particle size, chemical composition, light scattering, and density of ambient aerosols. The integrated light scattering measurements coupled with Mie theory could simultaneously retrieve aerosol refractive index and effective density. The combination of DMA and SPAMS could obtain effective densities as a function of particle sizes. This study extends the measurements of SPAMS to the microphysical properties and provides methods for multi-dimensional characterization of aerosols.

Acknowledgements *This work was supported by the "Strategic Priority Research Program (B)" of the Chinese Academy of Sciences (Grant No. XDB05020205), the National Natural Science Foundation of China (Grant No. 41405131), and the China Postdoctoral Science Foundation (Grant No. 2014M550442). This is contribution No. IS-2102 from GIGCAS.*

References

Buzorius G, Zelenyuk A, Brechtel F, Imre D. 2002. Simultaneous determination of individual ambient particle size, hygroscopicity and composition. Geophys Res Lett, 29: 1974, doi: 10.1029/2001GL014221

Bzdek B R, Pennington M R, Johnston M V. 2012. Single particle chemical analysis of ambient ultrafine aerosol: A review. J Aerosol Sci, 52: 109–120

Creamean J M, Suski K J, Rosenfeld D, Cazorla A, DeMott P J, Sullivan R C, White A B, Ralph F M, Minnis P, Comstock J M, Tomlinson J M, Prather K A. 2013. Dust and biological aerosols from the Sahara and Asia influence precipitation in the Western U.S. Science, 339: 1572–1578

DeCarlo P F, Slowik J G, Worsnop D R, Davidovits P, Jimenez J L. 2004. Particle morphology and density characterization by combined mobility and aerodynamic diameter measurements. Aerosol Sci Tech, 38: 1185–1205

Hand J L, Kreidenweis S M. 2002. A new method for retrieving particle refractive index and effective density from aerosol size distribution data. Aerosol Sci Tech, 36: 1012–1026

He J J, Zhang G H, Wang B G, Chen D H, Bi X H, Zhong L J, Sheng G Y, Fu J M, Zhou Z, Li L. 2013. Analysis of single particle characteristics during haze events in Heshan (in Chinese). Acta Sci Circum, 33: 2098–2104

Huang Z X, Gao W, Dong J G, Li L, Nian H Q, Fu Z, Zhou Z. 2010. Development of a real-time single particle aerosol time-of-flight mass spectrometer (in Chinese). J Chin Mass Spec Soc, 31: 332–341

Khlystov A, Stanier C, Pandis S N. 2004. An algorithm for combining electrical mobility and aerodynamic size distributions data when measuring ambient aerosol. Aerosol Sci Tech, 38: 229–238

Lee S H, Allen H C. 2012. Analytical measurements of atmospheric urban aerosol. Anal Chem, 84: 1196–1201

Li L, Huang Z X, Dong J G, Li M, Gao W, Nian H Q, Fu Z, Zhang G H, Bi X H, Cheng P, Zhou Z. 2011. Real time bipolar time-of-flight mass spectrometer for analyzing single aerosol particles. Int J Mass Spectrom, 303: 118–124

Li L, Tan G B, Zhang L, Fu Z, Nian H Q, Huang Z X, Zhou Z, Li M. 2013. Analysis of diesel exhaust particles using single particle aerosol mass spectrometry (in Chinese). Chin J Anal Chem, 41: 1831–1836

Liang F, Zhang N Z, Wang B, Hou K Y, Qu H B, Li H Y. 2005. Mass spectrometer for online analysis of size and chemical composition of single atmospheric particles (in Chinese). J Chin Mass Spec Soc, 26: 193–197

Lin Z J, Tao J, Chai F H, Fan S J, Yue J H, Zhu L H, Ho K F, Zhang R J. 2013. Impact of relative humidity and particles number size distribution on aerosol light extinction in the urban area of Guangzhou. Atmos Chem Phys, 13: 1115–1128

Moffet R C, Prather K A. 2005. Extending ATOFMS measurements to include refractive index and density. Anal Chem, 77: 6535–6541

Moffet R C, Qin X Y, Rebotier T, Furutani H, Prather K A. 2008. Chemically segregated optical and microphysical properties of ambient aerosols measured in a single-particle mass spectrometer. J Geophys Res, 113: 1–11

Pöschl U. 2005. Atmospheric aerosols: Composition, transformation, climate and health effects. Angew Chem-Int Edit, 44: 7520–7540

Prather K A, Nordmeyer T, Salt K. 1994. Real-time characterization of individual aerosol-particles using time-of-flight mass spectrometry. Anal Chem, 66: 1403–1407

Pratt K A, Prather K A. 2009. Real-time, single particle volatility, size, and chemical composition measurements of aged urban aerosols. Environ Sci Technol, 43: 8276–8282

Pratt K A, Prather K A. 2012. Mass spectrometry of atmospheric aerosols Recent developments and applications. Part II: On-line mass spectrometry techniques. Mass Spectrom Rev, 31: 17–48

Spencer M T, Shields L G, Prather K A. 2007. Simultaneous measurement of the effective density and chemical composition of ambient aerosol particles. Environ Sci Technol, 41: 1303–1309

Sullivan R C, Prather K A. 2005. Recent advances in our understanding of atmospheric chemistry and climate made possible by on-line aerosol analysis instrumentation. Anal Chem, 77: 3861–3885

Van Gulijk C, Marijnissen J C M, Makkee M, Moulijn J A, Schmidt-Ott A. 2004. Measuring diesel soot with a scanning mobility particle sizer and an electrical low-pressure impactor: Performance assessment with a model for fractal-like agglomerates. J Aerosol Sci, 35: 633–655

Virtanen A, Ronkko T, Kannosto J, Ristimaki J, Makela J M, Keskinen J, Pakkanen T, Hillamo R, Pirjola L, Hameri K. 2006. Winter and summer time size distributions and densities of traffic-related aerosol particles at a busy highway in Helsinki. Atmos Chem Phys, 6: 2411–2421

Wang Z Y, Hao L Q, Zhou L Z, Guo X Y, Zhao W W, Fang L, Zhang W J. 2006. Real-time detection of individual secondary organic aerosol particle from photooxidation of toluene using aerosol time of flight mass spectrometer. Sci China Ser B-Chem, 49: 267–272

Xia Z, Fang L, Zheng H Y, Kong X H, Zhou L Z, Gu X J, Zhu Y, Zhang W J. 2004. Real time measurement of chemical compositions of individual aerosol particles (in Chinese). Chin J Anal Chem, 32: 973–976

Yang F, Chen H, Wang X N, Yang X, Du J F, Chen J M. 2009. Single particle mass spectrometry of oxalic acid in ambient aerosols in Shanghai: Mixing state and formation mechanism. Atmos Environ, 43: 3876–3882

Yang F, Chen H, Du J F, Yang X, Gao S, Chen J M, Geng F H. 2012. Evolution of the mixing state of fine aerosols during haze events in Shanghai. Atmos Res, 104: 193–201

Zelenyuk A, Cai Y, Chieffo L, Imre D. 2005. High precision density measurements of single particles: The density of metastable phases. Aerosol Sci Tech, 39: 972–986

Zelenyuk A, Cai Y, Imre D. 2006. From agglomerates of spheres to irregularly shaped particles: Determination of dynamic shape factors from measurements of mobility and vacuum aerodynamic diameters. Aerosol Sci Tech, 40: 197–217

Zelenyuk A, Imre D, Han J H, Oatis S. 2008. Simultaneous measurements of individual ambient particle size, composition, effective density, and hygroscopicity. Anal Chem, 80: 1401–1407

Zhang G H, Bi X H, Li L, Chan L Y, Li M, Wang X M, Sheng G Y, Fu J M, Zhou Z. 2013. Mixing state of individual submicron carbon–containing particles during spring and fall seasons in urban Guangzhou, China: A case study. Atmos Chem Phys, 13: 4723–4735

Zhu T, Shang J, Zhao D F. 2011. The roles of heterogeneous chemical processes in the formation of an air pollution complex and gray haze. Sci China Ser B-Chem, 54: 145–153